Figure S1: Absorption spectra showing the cluster evolution using alternate sequences. The spectra of the precursor violet absorbing and hybridized conjugates are indicated by dotted lines and solid lines, respectively. (A) T3-TT-S_B with 5 equivalents of S_{Bc} and (b) T3-S_C with 2 equivalents of S_{Cc}.

Figure S2: The favored stoichiometry of the violet-absorbing cluster was investigated by acquiring absorption spectra with varying concentrations of Ag^+. The oligonucleotide concentration was 90 μM with 0.5 equivalents of BH_4^- relative to Ag^+. In relation to the oligonucleotide concentration, the relative concentrations are 4 Ag^+ (solid red), 6 Ag^+ (solid blue), 8 Ag^+ (solid black), 10 Ag^+ (solid green), 12 Ag^+ (dashed black), and 14 Ag^+ (dotted black). Up to 10 Ag^+, absorption solely at 400 nm increases with the amount of Ag^+, indicating that a favored binding site becomes increasingly populated. Beyond this stoichiometry, new electronic transitions develop, indicating that the preferred binding is saturated and enabling access to new binding sites.

Figure S3: To acquire relative stoichiometries via atomic emission, the violet- and near-infrared-absorbing species were isolated by size exclusion chromatography. The mobile phase was a 10 mM citrate buffer at pH = 6.5 supplemented with 300 mM $NaClO_4$. In (A), a chromatogram for the violet-absorbing cluster bound to T3–T_2–S_A was acquired at 260 nm to comprehensively evaluate all DNA species in the sample. The faster eluting species has only absorbance at 260 nm while the proceeding peak exhibits absorbance at both 260 nm due to the DNA and at 400 nm due to the cluster (see spectrum in (B)). Gaussian fits were used to determine the proper time window to isolate the violet-absorbing conjugate. In (C), correspondence between the DNA- (dashed line) and cluster- (solid line) specific chromatograms indicates that the desired complex is isolated without interference. In (D), the chromatogram for the near infrared absorbing cluster complex with T3–T_2–S_A:S_{Ac} is clearly resolved because of its relatively large size. The cluster- and DNA-specific chromatograms show correspondence of the retention times using the absorbances at 730 nm and 260 nm, respectively, thus supporting the purity of this isolated fraction, whose spectrum is shown in (E).

Figure S4: Transformation from the violet to near-infrared cluster is driven by hybridization, as indicated by an inflection in the absorbance at 730 nm (left axis, crosses) as a function of the relative target:sensor concentration. The derivative plot (right axis, closed circles) highlights this stoichiometry.

Figure S5: (A) These spectra dissect the role of salt on the cluster transformation. In a relatively high salt buffer with 300 mM $NaClO_4$, the sensor retains its absorbance at 400 nm (violet spectrum), but hybridization induces conversion to the near-infrared species (dark red spectrum). Together with the results from Figure 2 in which the complement was added prior to the $NaClO_4$, these results demonstrate that both high salt and complement are needed to transform the violet absorbing cluster. (B) Similar spectral response in buffers with 200 mM $NaClO_4$ and $NaNO_3$ indicate that Na^+ promotes cluster transformation. The dashed and solid lines represent the spectra before and after adding the complement, respectively. (C) These spectra describe the effect of dilution on the spectral transformation. The solid dark red spectrum was acquired using 30 μM T3-T_2-S_A with 60 μM S_{Ac} in a cell with a 1 cm pathlength, and the dashed black spectrum was acquired using 0.30 μM T3-T_2-S_A with 0.60 μM S_{Ac} in a cell with a 10 cm pathlength. The absorbance of the former was scaled by 10 fold to account for its 10 fold higher absorbance. In the dilute sample, the lower absorbance at 730 nm and retention of the absorbance at 400 nm suggest that the spectral transformation is restrained at lower concentrations because sensor aggregation is inhibited.

Figure S6: (A) Fluorescence correlation analysis was used to measure the occupancy of the probe volume for solutions with various concentrations. The correlation function was modeled by incorporating a coupled dark electronic state and a diffusive component, and the contrast for this latter contribution is inversely related to the number of emitters in the optical probe volume. Concentrations were determined based on an optical probe volume that was calibrated with a solution with a known concentration of Cy7. Based on the linear variation of the occupancies with dilution, the concentration in the stock solution was

determined by extrapolation. (B) Based on the concentration determined from the correlation analysis, the extinction coefficient of the cluster was calculated using the absorbance at 730 nm.

Figure S7: (Top) The central peak in the triplet pattern in Figure 4b was isolated and subsequently chromatographically characterized. (Bottom) This sample was then heated at 50 ^{o}C for 15 mins, and subsequent recovery of the triplet pattern suggests that the dimer is linked via noncovalent interactions. The vertical line shows the correspondence between the retention times of the peaks associated with the isolated (top) and heated (bottom) fractions.

Figure S8: These spectra demonstrate how pH influences the cluster transformation with the following scheme: pH = 8, solid; pH = 9, dotted; pH = 10, dashed. Robust cluster development as high as pH = 10 indicates that protons do not significantly contribute to the stability of this aggregate. A contributing factor to the progressive attenuation of the near infrared absorbance may be related to the favorability of forming silver oxide at higher pH.

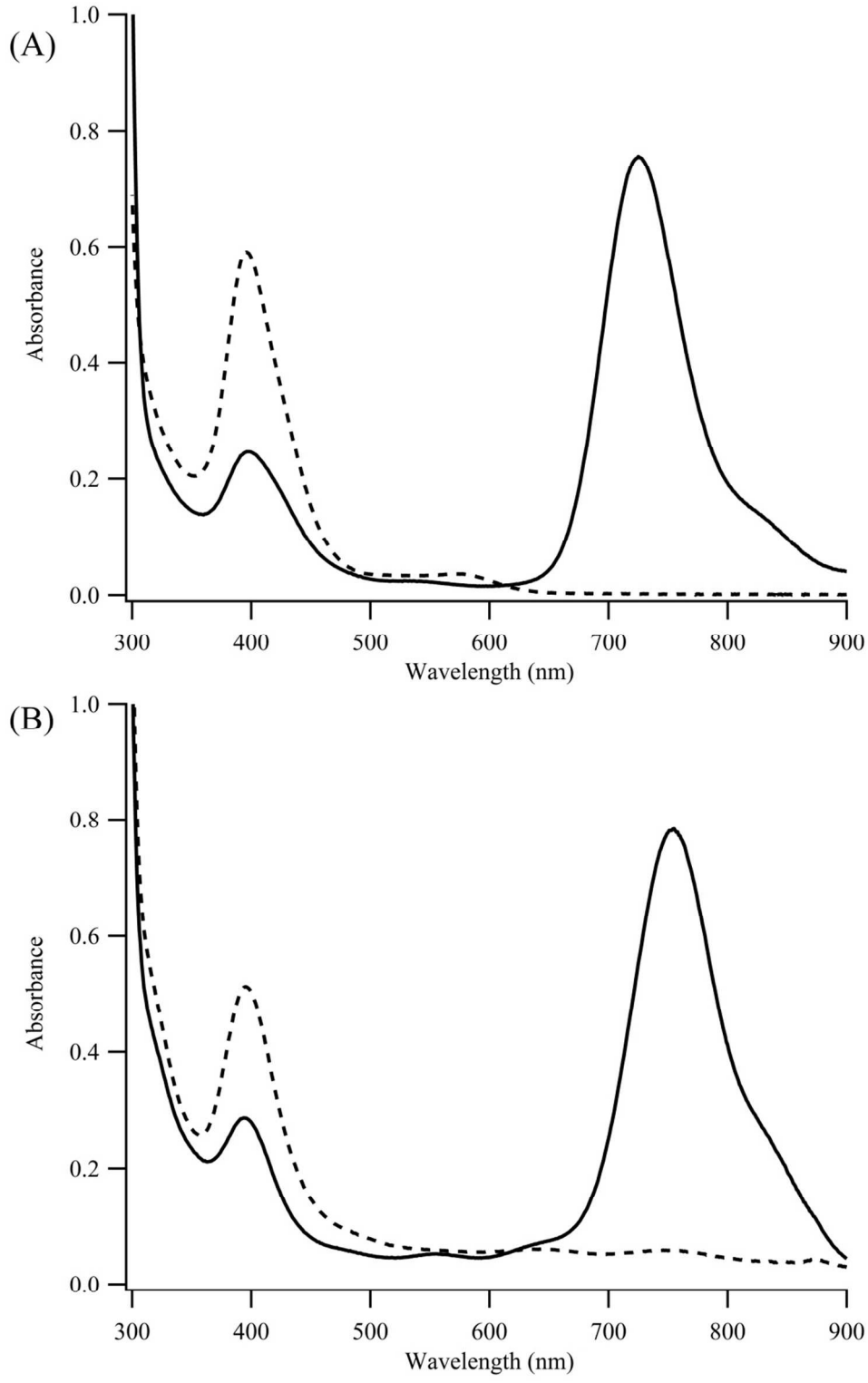
(A)
Absorbance
1.0
0.8
0.6
0.4
0.2
0.0
300
400
500
600
700
800
900
Wavelength (nm)
(B)
Absorbance
1.0
0.8
0.6
0.4
0.2
0.0
300
400
500
600
700
800
900
Wavelength (nm)

Figure S1

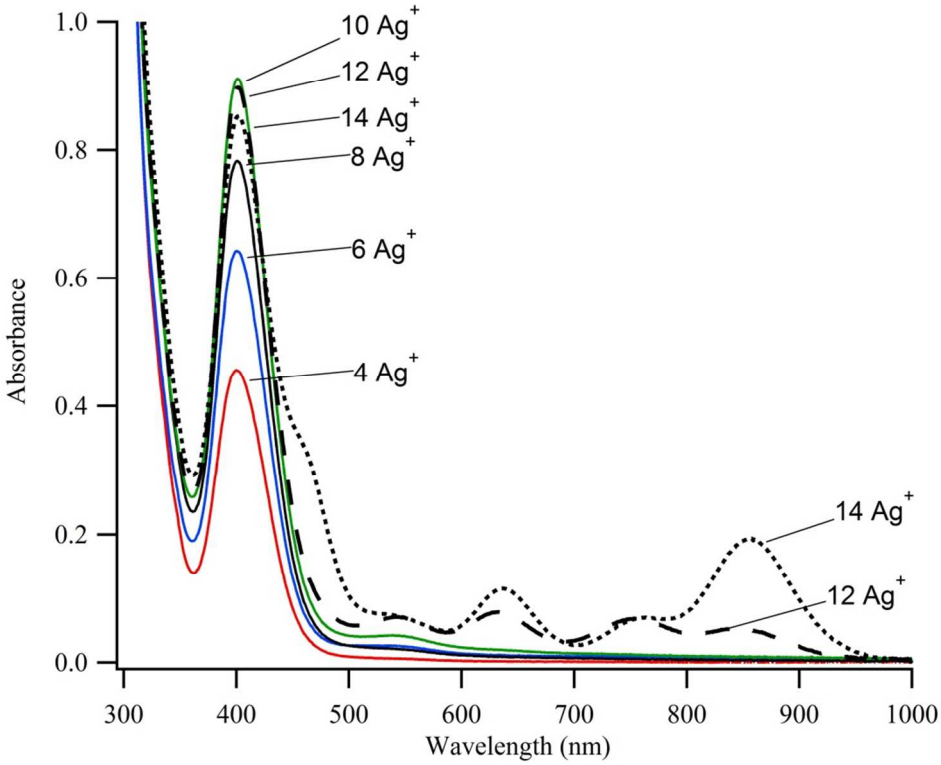
1.0
0.8
0.6
0.4
0.2
0.0
Absorbance
300
400
500
600
700
800
900
1000
Wavelength (nm)
10 Ag+
12 Ag+
14 Ag+
8 Ag+
6 Ag+
4 Ag+
14 Ag+
12 Ag+

Figure S2

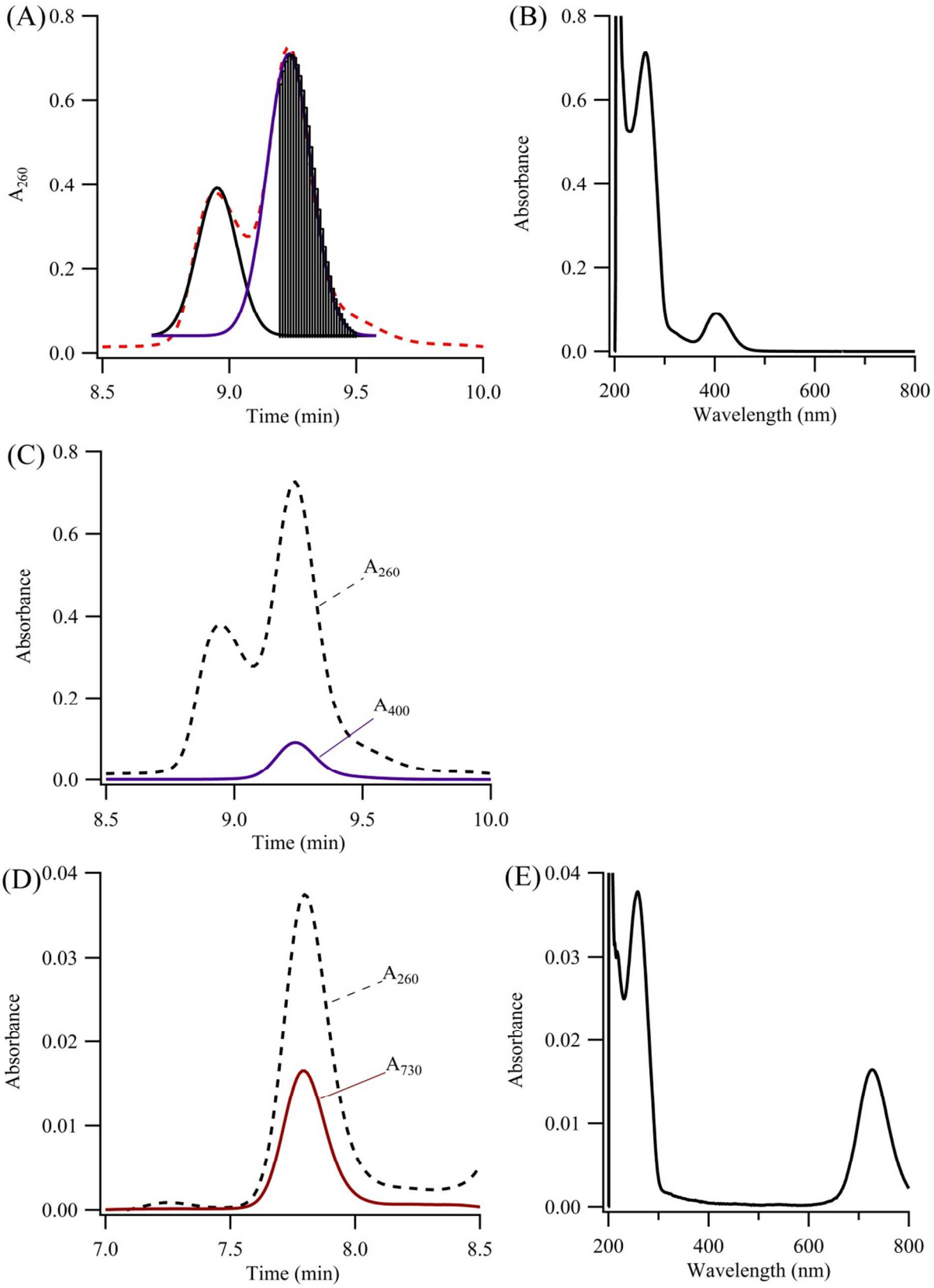
(A)
A260
Time (min)
(B)
Absorbance
Wavelength (nm)
(C)
Absorbance
A260
A400
Time (min)
(D)
Absorbance
A260
A730
Time (min)
(E)
Absorbance
Wavelength (nm)

Figure S3

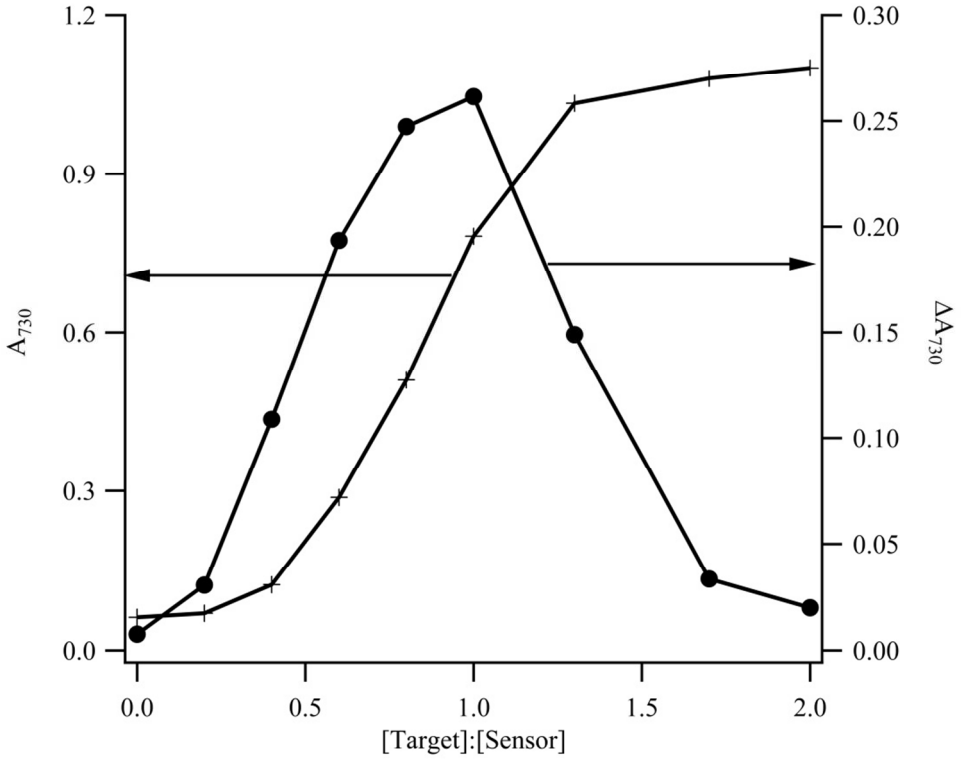
1.2
0.9
0.6
0.3
0.0
A730
0.30
0.25
0.20
0.15
0.10
0.05
0.00
ΔA730
0.0
0.5
1.0
1.5
2.0
[Target]:[Sensor]

Figure S4

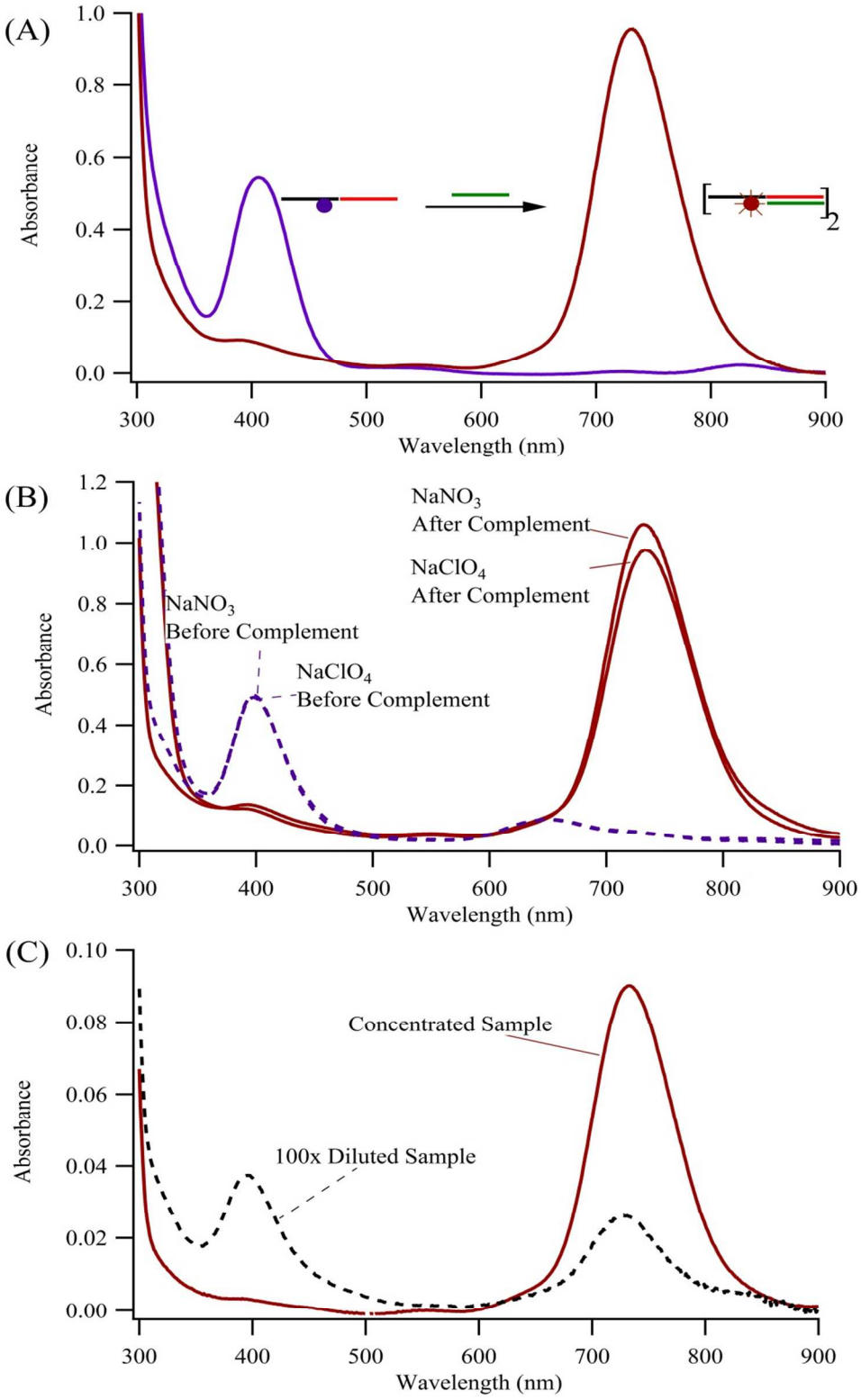
(A)
Absorbance
Wavelength (nm)
(B)
NaNO3
After Complement
NaClO4
After Complement
NaNO3
Before Complement
NaClO4
Before Complement
Absorbance
Wavelength (nm)
(C)
Concentrated Sample
100x Diluted Sample
Absorbance
Wavelength (nm)

Figure S5

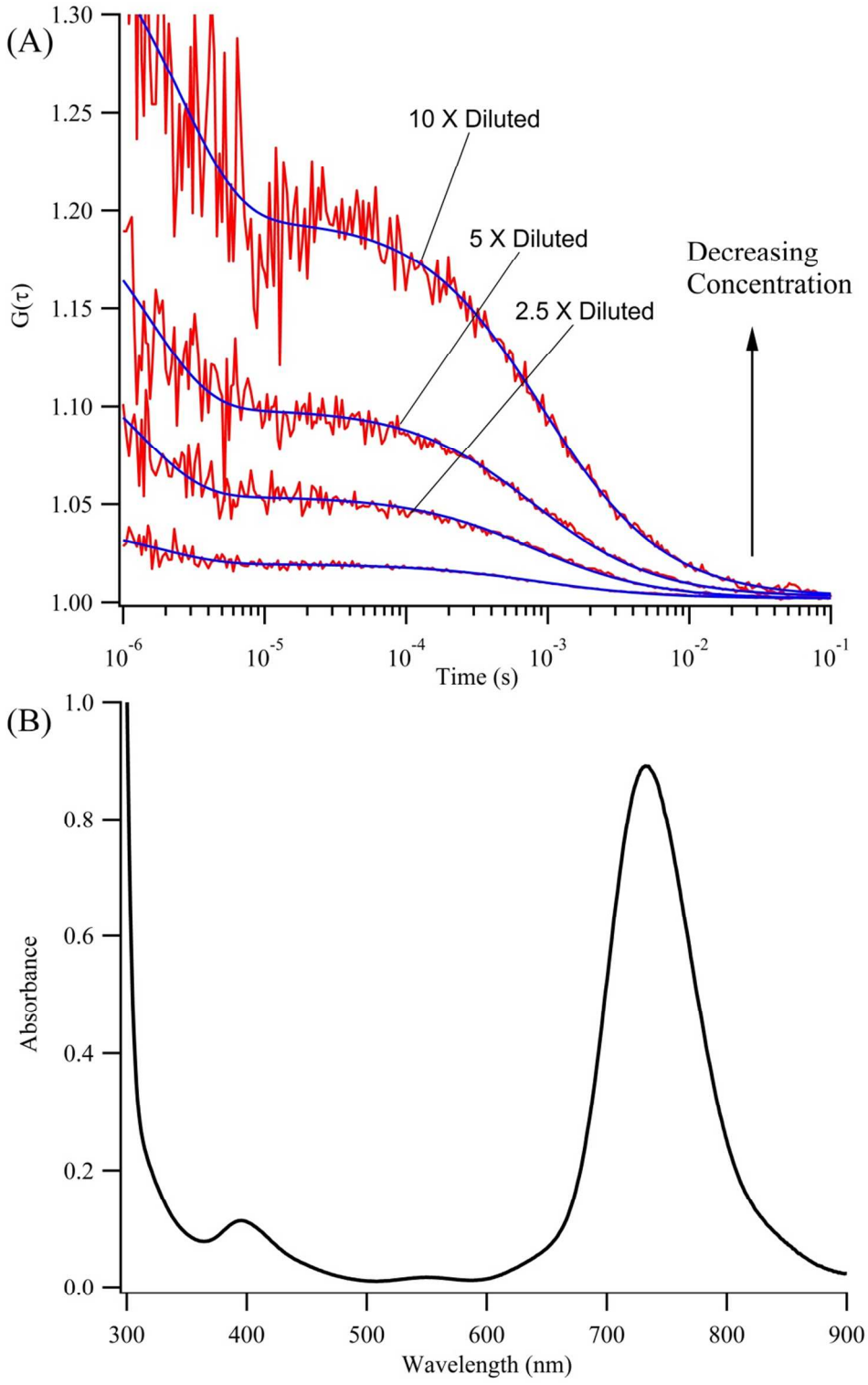
(A)
10 X Diluted
5 X Diluted
2.5 X Diluted
Decreasing
Concentration
G(τ)
Time (s)
(B)
Absorbance
Wavelength (nm)

Figure S6

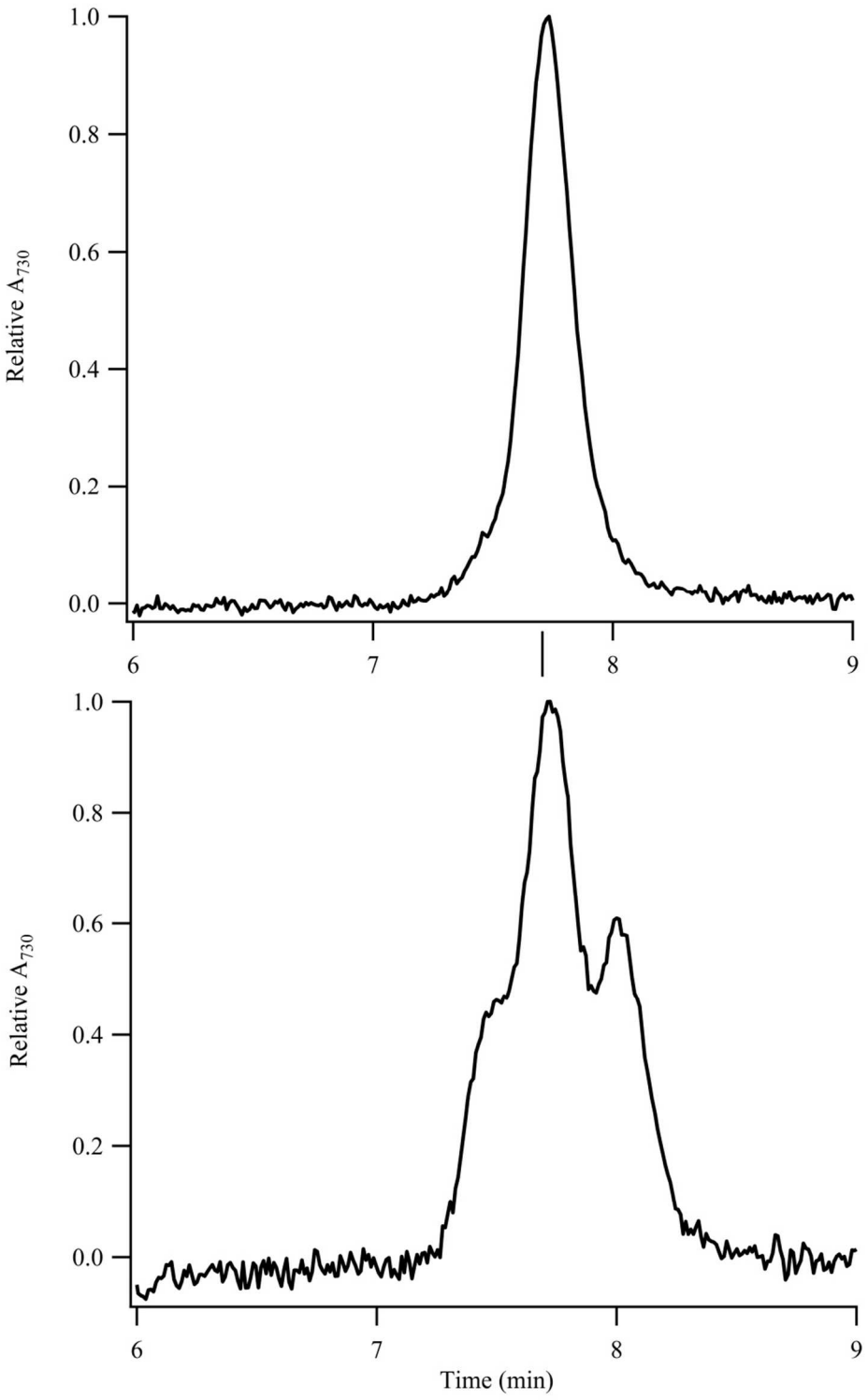
1.0
0.8
0.6
0.4
0.2
0.0
Relative A_{730}
6
7
8
9
1.0
0.8
0.6
0.4
0.2
0.0
Relative A_{730}
6
7
8
9
Time (min)

Figure S7

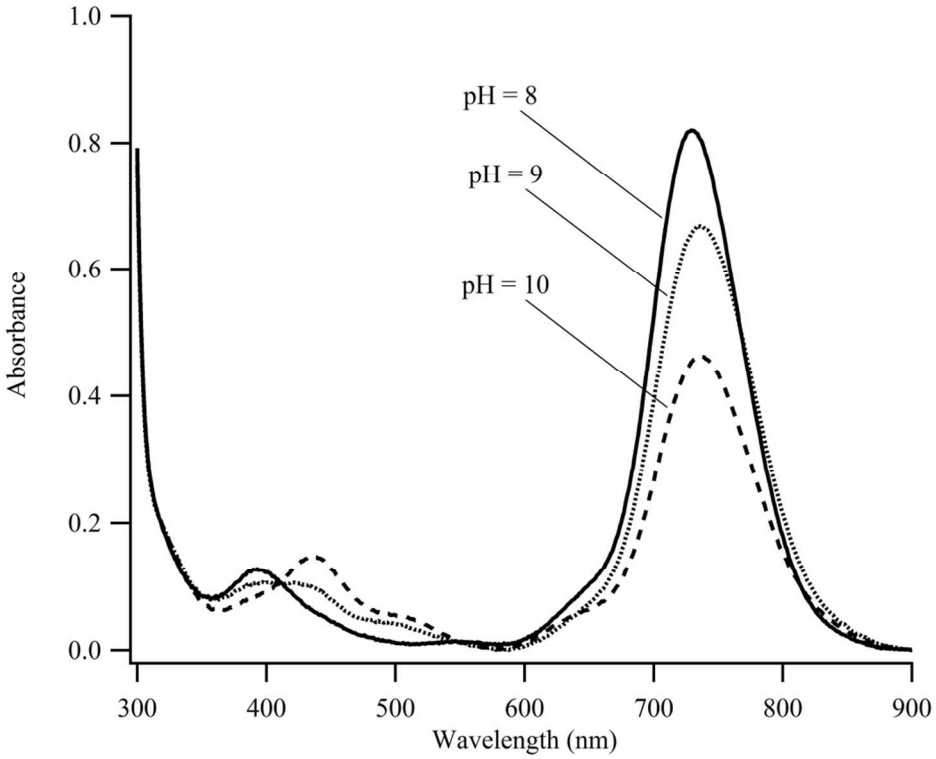
1.0
0.8
0.6
0.4
0.2
0.0
Absorbance
pH = 8
pII = 9
pH = 10
300
400
500
600
700
800
900
Wavelength (nm)

Figure S8